RAA 2018 Vol. **18** No. **4**, 39(8pp) doi: 10.1088/1674–4527/18/4/39

http://www.raa-journal.org *http://iopscience.iop.org/raa*

Research in Astronomy and Astrophysics

The effect of the equatorially symmetric zonal winds of Saturn on its gravitational field

Dali Kong[1,2], Keke Zhang[2,3], Gerald Schubert[4] and John D. Anderson[5]

[1] Key Laboratory of Planetary Sciences, Shanghai Astronomical Observatory, Chinese Academy of Sciences, Shanghai 200030, China
[2] College of Engineering, Mathematics and Physical Sciences, University of Exeter, Exeter, EX4 4QF, UK
[3] Lunar and Planetary Science Laboratory, Macau University of Science and Technology, Macau, China; *kzhang@ex.ac.uk*
[4] Department of Earth, Planetary and Space Sciences, University of California, Los Angeles, CA 90095-1567, USA
[5] Jet Propulsion Laboratory, 4800 Oak Grove Drive, Pasadena, CA 91109, USA

Received 2018 January 4; accepted 2018 February 6

Abstract The penetration depth of Saturn's cloud-level winds into its interior is unknown. A possible way of estimating the depth is through measurement of the effect of the winds on the planet's gravitational field. We use a self-consistent perturbation approach to study how the equatorially symmetric zonal winds of Saturn contribute to its gravitational field. An important advantage of this approach is that the variation of its gravitational field solely caused by the winds can be isolated and identified because the leading-order problem accounts exactly for rotational distortion, thereby determining the irregular shape and internal structure of the hydrostatic Saturn. We assume that (i) the zonal winds are maintained by thermal convection in the form of non-axisymmetric columnar rolls and (ii) the internal structure of the winds, because of the Taylor-Proundman theorem, can be uniquely determined by the observed cloud-level winds. We calculate both the variation $\Delta J_n, n = 2, 4, 6 \ldots$ of the axisymmetric gravitational coefficients J_n caused by the zonal winds and the non-axisymmetric gravitational coefficients ΔJ_{nm} produced by the columnar rolls, where m is the azimuthal wavenumber of the rolls. We consider three different cases characterized by the penetration depth $0.36\,R_{\rm S}, 0.2\,R_{\rm S}$ and $0.1\,R_{\rm S}$, where $R_{\rm S}$ is the equatorial radius of Saturn at the 1-bar pressure level. We find that the high-degree gravitational coefficient $(J_{12} + \Delta J_{12})$ is dominated, in all the three cases, by the effect of the zonal flow with $|\Delta J_{12}/J_{12}| > 100\%$ and that the size of the non-axisymmetric coefficients ΔJ_{mn} directly reflects the depth and scale of the flow taking place in the Saturnian interior.

Key words: gravitation — planets and satellites: individual (Saturn) — planets and satellites: interiors

1 INTRODUCTION

The generation and maintenance of Saturnian zonal winds remains a major scientific puzzle. They may be maintained by thermal convection, partly powered by internal heat, taking place within the deep interior of the planet (Busse 1976) or confined to a very thin top layer of a stably stratified Saturnian atmosphere (Ingersoll & Cuzzi 1969). If they are deep, the zonal winds would generate an externally measurable gravitational signature by inducing dynamic density anomalies (see, for example, Hubbard 1999). It is anticipated that the high-precision measurements carried out by the Cassini Grand Finale, together with accurate theoretical modeling, would resolve this long-term scientific puzzle. This study is concerned with the accurate modeling of the three-dimensional gravitational perturbation produced by the equatorially symmetric fluid motion in the interior of Saturn.

Spherical or spheroidal geometry, which is mathematically simple and computationally convenient, has been used to model the variation $\Delta J_{2n}, n = 1, 2, 3, \ldots$ of the even zonal gravitational coefficients J_{2n} caused by the effect of deep zonal winds in giant planets.

Hubbard (1999) computed ΔJ_{2n} for a spherical Jupiter in which the cloud-level, equatorially symmetric zonal winds extend all the way on cylinders from the northern to the southern hemisphere; Kaspi et al. (2010) calculated ΔJ_{2n} for a spherical Jupiter using the thermal-wind equation by assuming that the observed cloud-level winds extend on cylinders but decay exponentially in the radial direction; Liu et al. (2014) investigated, based on the thermal wind equation using the anelastic approximation, the relationship between the gravitational signals and the depth of the wind penetration for a spherical Saturn; Kong et al. (2013) computed the variation ΔJ_{2n} of the gravitational coefficients caused by the effect of zonal winds confined to cylinders inside an oblate spheroidal Jupiter.

Neither spherical nor oblate spheroidal geometries are adequate for interpreting the gravitational signals of Saturn produced by its equatorially symmetric zonal winds because of the irregular shape of the 1-bar pressure level. Both the wind-induced density anomaly and the rotational distortion contribute to the even zonal gravitational coefficients. In the measured coefficient $(J_{2n} + \Delta J_{2n})$, J_{2n} is caused by the rotational distortion in equilibrium under the balance of self-gravity, internal pressure and rotational effects while the correction ΔJ_{2n} is produced by the axially symmetric, equatorially symmetric zonal flow. Identifying the correction ΔJ_{2n}, which is usually small, from the measured value $(J_{2n} + \Delta J_{2n})$ represents a mathematically challenging problem and the assumption of either spherical or oblate spheroidal geometry used in the previous studies (see, for example, Hubbard 1999; Kong et al. 2013) must be removed from the modeling (Kong et al. 2016). The need for isolating a small correction ΔJ_{2n} from a measured value $(J_{2n} + \Delta J_{2n})$ leads to a self-consistent perturbation approach (Zhang et al. 2017) in which the leading-order solution accounts for the full effect of rotational distortion and determines the internal density profile $\rho(\boldsymbol{r})$, where $\boldsymbol{r}$ is the position vector, the irregular shape of a giant planet is described by $\mathcal{S}_{\rm o}(\boldsymbol{r})$ and the gravitational coefficients are J_{2n} in hydrostatic equilibrium while the next-order solution provides the correction ΔJ_{2n} that is solely caused by the effect of the zonal winds on the rotationally distorted planet. It is referred to as a self-consistent perturbation approach because two different problems resulting from the approach are mathematically and physically coupled and must be considered in a self-consistent way.

In the first paper of this series (Kong et al. 2018) on the gravitational field, shape and zonal winds of Saturn, we constructed a hydrostatic Saturnian model consisting of an ice-rock core, a metallic region, an outer molecular envelope and a thin transition layer between the metallic and molecular regions. The model, constrained by the known Saturnian gravitational field, produces an ice-rock core with equatorial radius $0.203\,R_{\rm S}$, where $R_{\rm S}$ is the equatorial radius of Saturn at the 1-bar pressure level, the core density $\rho_{\rm c} = 10388.1\,{\rm kg\,m^{-3}}$ corresponding to 13.06 Earth masses, an analytical expression describing the Saturnian irregular shape $\mathcal{S}_{\rm o}$ of the 1-bar pressure level and the internal density profile $\rho(\boldsymbol{r})$ of Saturn. The model also predicts the values of the higher-order gravitational coefficients, J_8, J_{10} and J_{12} and suggests that Saturn's convective dynamo operates in the metallic region approximately defined by $0.2\,R_{\rm S} < r_e < 0.7\,R_{\rm S}$, where r_e denotes the equatorial radial distance from the center of figure. The hydrostatic Saturnian model provides the required framework so that the effect of the equatorially symmetric zonal winds on its gravitational field can be understood.

In this paper, we adopt the self-consistent perturbation approach for the gravitational sounding of an equatorially symmetric fluid motion $\boldsymbol{u}(\boldsymbol{r})$ that may occur in the molecular envelope of Saturn. The perturbation expands the total pressure $p_{\rm total}(\boldsymbol{r})$, the total density anomaly $\rho_{\rm total}(\boldsymbol{r})$, the measured 1-bar pressure surface $\mathcal{S}$ and the total gravitational potential $V_{\rm total}(\boldsymbol{r})$ in the form

$$p_{\rm total}(\boldsymbol{r}) = p(\boldsymbol{r}) + p'(\boldsymbol{r}), \tag{1}$$

$$\rho_{\rm total}(\boldsymbol{r}) = \rho(\boldsymbol{r}) + \rho'(\boldsymbol{r}), \tag{2}$$

$$V_{\rm total}(\boldsymbol{r}) = V_{\rm g}(\boldsymbol{r}) + V'(\boldsymbol{r}), \tag{3}$$

$$\mathcal{S}_{\rm measured}(\boldsymbol{r}) = \mathcal{S}_{\rm o}(\boldsymbol{r}) + \mathcal{S}'(\boldsymbol{r}), \tag{4}$$

where the leading-order solution $(p, \rho, V_{\rm g}, \mathcal{S}_{\rm o})$, which is discussed in Kong et al. (2018), represents the hydrostatic equilibrium state (i.e., when $\boldsymbol{u}(\boldsymbol{r}) = \boldsymbol{0}$ in the rotating frame of reference) while $(p', \rho', V', \mathcal{S}')$ denotes the perturbation that arises from the effect of the fluid motion $\boldsymbol{u}(\boldsymbol{r})$ and will be identified in this study.

An important question then is what is the structure and amplitude of the equatorially symmetric fluid motion $\boldsymbol{u}(\boldsymbol{r})$ in the interior of Saturn about which we know very little. Although significant progress has been made in modeling the zonal winds on giant planets driven by thermal convection (see, for example, Busse 1976; Heimpel et al. 2005; Jones & Kuzanyan 2009; Gastine & Wicht 2012), achieving the realistic physical parameters will probably never be possible for Saturn and extrapolating the solutions from a numerically accessible model over many orders of magnitude is unreliable. We therefore have to infer the key characteristics of $\boldsymbol{u}(\boldsymbol{r})$ from the existing observations together with our theoretical understanding of the problem. Because of the dynamical control by rotational effects, the flow $\boldsymbol{u}(\boldsymbol{r})$ in the Saturnian molecular envelope is nearly geostrophic, leading to an axially symmetric, equatorially symmetric zonal flow on cylinders parallel to the rotation axis. It follows that the structure and amplitude of the deep zonal flow in the molecular region can be uniquely determined by making use of the structure and amplitude of the observed cloud-level zonal winds. But the zonal flow must be sustained via the axially non-symmetric fluid motion in the form of columnar rolls which are also quasi-geostrophic (see, for example, Busse 1976; Jones & Kuzanyan 2009). Through the effects of rapid rotation and the planet's curvature, the rolls become spiralling and highly correlated and, hence, are capable of generating a strong zonal flow whose amplitude can be much larger than that of the rolls (Zhang 1992). At present, we do not know the structure and amplitude of the convective rolls in the Saturnian interior. Consequently, a parameterized model has to be adopted for the non-axisymmetric component of convection. If the axially non-symmetric gravitational signals are detected by Cassini Grand Finale, the physical parameters of the rolls, such as the dominant azimuthal wavenumber, can be estimated using our fully three-dimensional model. This is the first time that a gravitational inverse model for giant planets includes both an axially symmetric and equatorially symmetric zonal flow on cylinders and an axially non-symmetric and equatorially symmetric flow in the form of columnar rolls.

In what follows we begin by presenting the model of Saturn and the mathematical formulation in Section 2, which is followed by discussion of the results in Section 3 with a summary and some remarks given in Section 4.

2 MODEL AND FORMULATION

Our Saturnian model assumes that (i) Saturn with mass M_{S} is isolated and rotating about the z-axis with the angular velocity $\Omega_{\mathrm{S}} = 1.65434 \times 10^{-4}\,\mathrm{s}^{-1}$ (Helled et al. 2015); (ii) the equation of state of the gases in the molecular envelope (assumed to be polytropic) is determined by the leading-order hydrostatic problem (Kong et al. 2018); (iii) there exists the fluid motion $\boldsymbol{u}(\boldsymbol{r})$ relative to the rotating frame of reference expressible in the form

$$\boldsymbol{u}(r,\theta,\phi) = U_\phi(r,\theta)\hat{\boldsymbol{\phi}} + \boldsymbol{U}(r,\theta,\phi),$$

where (r,θ,ϕ) are spherical polar coordinates with the corresponding unit vectors $(\hat{\boldsymbol{r}},\hat{\boldsymbol{\theta}},\hat{\boldsymbol{\phi}})$ and $\theta = 0$ is at the axis of rotation, $U_\phi(r,\theta)\hat{\boldsymbol{\phi}}$ denotes the axially symmetric and equatorially symmetric zonal flow and $\boldsymbol{U}(r,\theta,\phi)$ represents the velocity of columnar convective rolls; (iv) the Rossby number of the fluid motion $\boldsymbol{u}(\boldsymbol{r})$ is small and the Ekman number is also negligibly small; and (v) the large-scale fluid motion $\boldsymbol{u}(\boldsymbol{r})$ is in a statistically steady state. The assumption of the steady flow is based on the following reasons: the profile of the observed Saturnian zonal winds has largely remained unchanged over many decades (García-Melendo et al. 2011) and the numerical simulations of rotating convection (see, for example, Jones & Kuzanyan 2009) suggest that the large-scale fluid motion such as the mean zonal flow, sustained by the spatially small-scale and temporally fluctuating flow, is typically in a statistically steady state. A sketch of the axially symmetric zonal flow in the molecular envelope is shown in Figure 1(a) while a sketch of the non-axisymmetric convective rolls is depicted in Figure 1(b).

Substitution of the expansion, defined in Equations (1)–(4), into the governing equations in the rotating frame of reference leads to two different but mathematically coupled problems. The leading-order problem for the fluid region $\mathcal{D}_{\mathrm{o}}$ of Saturn is governed by the equations

$$0 = -\frac{1}{\rho(\boldsymbol{r})}\nabla p(\boldsymbol{r}) - \nabla V_{\mathrm{g}}(\boldsymbol{r}) - \frac{\Omega_{\mathrm{S}}^2}{2}\nabla|\hat{\boldsymbol{z}}\times\boldsymbol{r}|^2, \tag{5}$$

$$p(\boldsymbol{r}) = K(\boldsymbol{r})\rho(\boldsymbol{r})^{1+\frac{1}{n(\boldsymbol{r})}}, \tag{6}$$

$$\nabla^2 V_{\mathrm{g}}(\boldsymbol{r}) = 4\pi G\rho(\boldsymbol{r}), \tag{7}$$

where $K(\boldsymbol{r})$ and $n(\boldsymbol{r})$ mean that they are functions of $\boldsymbol{r}$ in the fluid region, $p(\boldsymbol{r})$ is the pressure, $\rho(\boldsymbol{r})$ is the density and $V_{\mathrm{g}}(\boldsymbol{r})$ is the gravitational potential. Equations (5)–(7) are solved subject to the two boundary conditions at the 1-bar pressure surface $\mathcal{S}_{\mathrm{o}}$

$$[p]_{|\boldsymbol{r}|=\mathcal{S}_{\mathrm{o}}} = 1\,\mathrm{bar}, \tag{8}$$

$$G\left[\iiint_{\mathcal{D}_{\mathrm{c}}}\frac{\rho_{\mathrm{c}}\,\mathrm{d}^3\boldsymbol{r}'}{|\boldsymbol{r}-\boldsymbol{r}'|} + \iiint_{\mathcal{D}_{\mathrm{o}}}\frac{\rho(\boldsymbol{r}')\,\mathrm{d}^3\boldsymbol{r}'}{|\boldsymbol{r}-\boldsymbol{r}'|} + \frac{\Omega_{\mathrm{S}}^2}{2}|\hat{\boldsymbol{z}}\times\boldsymbol{r}|^2\right]_{|\boldsymbol{r}|=\mathcal{S}_{\mathrm{o}}} = \text{constant}, \tag{9}$$

where ρ_{c} is the density of the ice-rock core, $\mathcal{D}_{\mathrm{c}}$ represents the domain of the core, $[\mathcal{F}]_{|\boldsymbol{r}|=\mathcal{S}_{\mathrm{o}}}$ denotes the evaluation of a function $\mathcal{F}$ at the 1-bar pressure surface $\mathcal{S}_{\mathrm{o}}$ and $\iiint_{\mathcal{D}}\mathrm{d}^3\boldsymbol{r}'$ represents the volume integration over the domain $\mathcal{D}$. The results of the leading-order hydrostatic solution, such as the shape $\mathcal{S}_{\mathrm{o}}$ and the density $\rho(\boldsymbol{r})$, are discussed in Kong et al. (2018).

The next-order problem arising from the self-consistent perturbation approach, which describes the density anomaly $\rho'(\boldsymbol{r})$ induced by the fluid motion $\boldsymbol{u}(\boldsymbol{r})$,

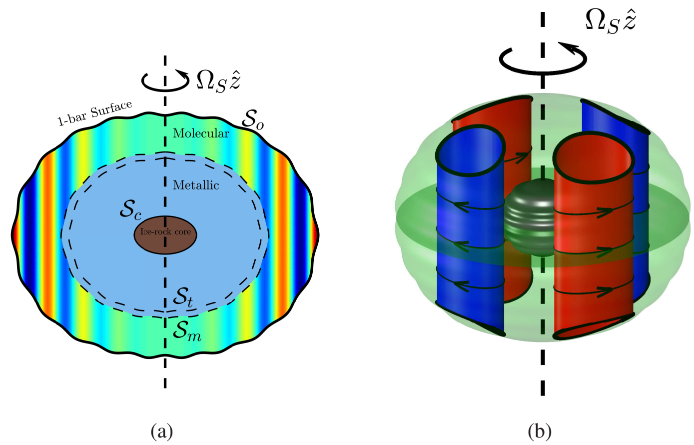

Fig. 1 (a) Sketch of the Saturnian model in a meridional plane: an ice-rock core, a metallic hydrogen-helium dynamo region, an outer molecular insulating envelope and a thin metallic–molecular transition layer. The axially symmetric and equatorially symmetric zonal flow is confined in the molecular envelope between the *irregular* 1-bar-pressure surface $\mathcal{S}_\mathrm{o}$ and an *irregular* constant density surface determined by the leading-order problem. (b) Sketch of the non-axisymmetric columnar rolls with the azimuthal wavenumber $m = 2$ producing the non-axisymmetric gravitational signals.

is governed by the equations

$$2\Omega_\mathrm{S}\hat{\boldsymbol{z}} \times \left[U_\phi(r,\theta)\hat{\boldsymbol{\phi}} + \boldsymbol{U}(\boldsymbol{r})\right] = -K\left(1+\frac{1}{n}\right) \times \left[\frac{1-n}{n}\left(\rho^{\frac{(1-2n)}{n}}\boldsymbol{\nabla}\rho\right)\rho' + \rho^{\frac{(1-n)}{n}}\nabla\rho'\right] - \boldsymbol{\nabla}V'(\boldsymbol{r}), \qquad (10)$$

$$\boldsymbol{\nabla}^2 V'(\boldsymbol{r}) = 4\pi G\rho'(\boldsymbol{r}), \qquad (11)$$

$$\boldsymbol{\nabla}\cdot\left\{\left[U_\phi(r,\theta)\hat{\boldsymbol{\phi}} + \boldsymbol{U}(\boldsymbol{r})\right\}\rho(\boldsymbol{r})\right] = 0, \qquad (12)$$

subject to the two boundary conditions

$$[\rho'(\boldsymbol{r})]_{|\boldsymbol{r}|=\mathcal{S}_\mathrm{o}} = 0 \text{ and } [\rho'(\boldsymbol{r})]_{|\boldsymbol{r}|=\mathcal{S}_\mathrm{b}} = 0, \qquad (13)$$

where $\mathcal{S}_\mathrm{o}$ denotes the irregular 1-bar pressure surface, $K = K_2 = 246678.9\,\mathrm{Pa\,m^6\,kg^{-2}}$, $n = n_2 = 1.0725$ for the polytropic law in the molecular region and $\rho(\boldsymbol{r})$ is the hydrostatic density, all of which are determined by the leading-order solution; $\mathcal{S}_\mathrm{b}$ represents an irregular constant density surface between $\mathcal{S}_\mathrm{m}$ and $\mathcal{S}_\mathrm{o}$ whose equatorial radius is R_H. Since n is very close to unity, it is expected that the term with the coefficient $(1-n)/n$ in Equation (10) is insignificant. The fluid motion $[U_\phi(r,\theta)\hat{\boldsymbol{\phi}} + \boldsymbol{U}(r,\theta,\phi)]$ is assumed to be confined between $\mathcal{S}_\mathrm{o}$ and $\mathcal{S}_\mathrm{b}$, and the location of the surface $\mathcal{S}_\mathrm{b}$, characterized by the size of its equatorial radius R_H, will be treated as the depth parameter.

The small-shape perturbation caused by the effect of the zonal winds is neglected at this order and, consequently, the true surface $\mathcal{S} = \mathcal{S}_\mathrm{o} + \mathcal{S}'$ under the influence of $\boldsymbol{u}(\boldsymbol{r})$ is unknown at this order of the analysis. This also implies that the total mass, the solution

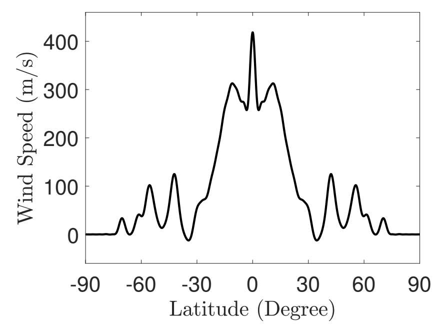

Fig. 2 The latitudinal profile of the equatorially symmetric zonal winds at the Saturnian 1-bar pressure level (García-Melendo et al. 2011) used in our model.

of Equations (10)–(12) subject to Equation (13), is not conserved. In contrast to the thermal-wind-balance approach, the boundary conditions from Equation (13) for $\rho'(\boldsymbol{r})$ are not only necessary but also play an important role in determining the structure of the solution.

For a prescribed three-dimensional fluid motion $\boldsymbol{u}(\boldsymbol{r})$ together with the solution of the leading-order Equations (5)–(7), we solve Equations (10)–(12) subject to the conditions in Equations (13), using a three-dimensional finite element method based on a three-dimensional tetrahedralization of the irregular solution domain (Kong et al. 2016), to determine the density anomaly $\rho'(\boldsymbol{r})$ and, hence, the variation of the Saturnian gravitational field solely produced by the effect of the prescribed flow $\boldsymbol{u}(\boldsymbol{r})$. For the results reported in this paper, the irregular solution domain of Saturn is typically divided into about 10^7 tetrahedral elements. Moreover, we have also computed our numerical solutions at different levels of the resolution to ensure convergence of the solutions.

3 RESULTS AND DISCUSSIONS

The gravitational potential perturbation V' in the exterior of a rotationally distorted Saturn, if its interior flow $\boldsymbol{u}(\boldsymbol{r})$ is equatorially symmetric, can be expanded in the form

$$V'(r,\theta,\phi) = -\frac{GM_{\rm S}}{r}\left[1-\sum_{n=2}^{\infty}\left(\frac{R_{\rm S}}{r}\right)^n \Delta J_n P_n(\cos\theta) - \sum_{n=2}^{\infty}\sum_{m=1}^{n}\left(\frac{R_{\rm S}}{r}\right)^n P_{nm}(\cos\theta) \times (C_{nm}\cos m\phi + S_{nm}\sin m\phi)\right], \quad (14)$$

where $M_{\rm S}$ is Saturn's mass and $GM_{\rm S} = 3.7931 \times 10^{16}\,{\rm m^3\,s^{-2}}$ (Williams 2016), n takes even integers, $\Delta J_2, \Delta J_4, \Delta J_6, \ldots,$ are the variation of the axisymmetric gravitational coefficients produced by the axially symmetric zonal winds $U_\phi(r,\theta)$ while (C_{nm}, S_{nm}) are the non-axisymmetric gravitational coefficients caused by the convective rolls $\boldsymbol{U}(r,\theta,\phi)$. In Equation (14), the associated Legendre polynomials are normalized as

$$\int_{-1}^{1} P_{nm}(\mu)P_{n'm}(\mu)\mathrm{d}\mu = \frac{2(n+m)!}{(2n+1)(n-m)!}\delta_{n,n'}. \quad (15)$$

For convenience of discussion, we define

$$J_{nm} = \sqrt{C_{nm}^2 + S_{nm}^2}$$

which measures the strength of the non-axisymmetric gravitational field.

For the the axially symmetric zonal flow, we extend the observed cloud-level zonal winds, shown in Figure 2, on cylinders parallel to the rotation axis from the 1-bar pressure level to the constant density surface $\mathcal{S}_{\rm b}$ with its equatorial radius R_H. In this way, both the amplitude and the structure of $U_\phi(r,\theta)$ in Equation (10) are uniquely determined. For the non-axisymmetric columnar rolls, we take a parameterized convection model

$$\boldsymbol{U} = \mathcal{U}_0\left[\hat{\boldsymbol{s}}\frac{f(s)}{s}\cos(m\phi) - \hat{\boldsymbol{\phi}}\frac{1}{m}\frac{\partial f}{\partial s}\sin(m\phi)\right], \quad (16)$$

where $\mathcal{U}_0$ represents the typical speed of the columnar convective rolls confined between the constant density surface $\mathcal{S}_{\rm b}$ and the 1-bar pressure surface $\mathcal{S}_{\rm o}$, m is the azimuthal wavenumber of the rolls, $s = (r\sin\theta)/R_{\rm S}$, $f(s) = s^3\sin(2\pi s)$ and $\hat{\boldsymbol{s}}$ denotes the unit vector perpendicular to the rotation axis. This parameterized non-axisymmetric flow approximately satisfies Equation (12) and mimics the dynamically possible structure of thermal convection under the strong rotational influence (Busse 1976; Zhang & Schubert 2000; Jones & Kuzanyan 2009). In this study, we take $\mathcal{U}_0 = 10\,{\rm m\,s^{-1}}$ and $m = 2$ for the purpose of illustration; the parameters of the convective flow in our model can be readily changed if the high-precision measurements by the Cassini Grand Finale suggest a different structure.

We first discuss the effect of the axially symmetric zonal flow on the Saturnian gravitational field. Since the leading-order solution has already taken account of the full effect of rotational distortion, the variation ΔJ_n, which is related to the solution $\rho'(\boldsymbol{r})$ of Equations (10)–(11), is solely caused by the effect of the zonal flow. Consider the three different cases: (i) a very deep wind profile with $R_H = 0.664\,R_{\rm S}$, (ii) an intermediate deep profile with $R_H = 0.8\,R_{\rm S}$ and (iii) a shallow profile with $R_H = 0.90\,R_{\rm S}$. Whereas the surface $\mathcal{S}_{\rm b}$ marked by $R_H = 0.6641\,R_{\rm S}$ corresponds to the metallic–molecular interface $\mathcal{S}_{\rm m}$ determined by the leading-order solution, the other two cases are considered because the outer layer of the molecular region may be stably stratified or because the zonal flow in the Saturnian interior may be blocked by the effect of its magnetic field if its electrical conductivity becomes sufficiently high (Liu et al. 2008).

The density anomaly $\rho'(\boldsymbol{r})$ produced by a deep zonal flow with $R_H = 0.664\,R_{\rm S}$ is depicted in Figure 3, showing that the maximum amplitude of the anomaly is about $8\,{\rm kg\,m^{-3}}$ in the equatorial region and that the density anomalies ρ' are primarily negative. Modified by the boundary conditions required on both the surfaces $\mathcal{S}_{\rm m}$ and $\mathcal{S}_{\rm o}$, the distribution of density anomaly $\rho'(\boldsymbol{r})$ largely reflects the cylindrical structure of the zonal winds. Figure 3 also shows that the density anomaly $\rho'(\boldsymbol{r})$ occurs mainly in the equatorial region, which is expected since the zonal winds in Figure 2 have the largest amplitude there. It should be highlighted that the shapes of $\mathcal{S}_{\rm m}$ and $\mathcal{S}_{\rm o}$ in Figure 3 are non-spheroidal and irregular but their deviations from oblate spheroids are too small to be noticeable in the figure. After obtaining the density anomaly $\rho'(\boldsymbol{r})$, we can then compute the variation ΔJ_n caused by the zonal winds via the following integration

$$\Delta J_n = -\frac{(2n+1)R_{\rm S}}{2M_{\rm S}} \times \int_0^{\pi}\left[\iiint_{\mathcal{D}_{\rm b}}\frac{\rho'(\boldsymbol{r}')\,\mathrm{d}^3\boldsymbol{r}'}{|\boldsymbol{r}-\boldsymbol{r}'|}\right]_{|\boldsymbol{r}|=R_{\rm S}} \times P_n(\cos\theta)\,\sin\theta\,\mathrm{d}\theta, \quad (17)$$

where the domain $\mathcal{D}_{\rm b}$ represents the region of the fluid motion. The result of this case, along with the other two cases, is presented in Table 1. Comparison between Table 1 and table 2 in Kong et al. (2018) reveals that,

Table 1 Variation ΔJ_n of the Axisymmetric Gravitational Coefficients J_n

R_H	$0.6641\,R_\mathrm{S}$	$0.8\,R_\mathrm{S}$	$0.9\,R_\mathrm{S}$
$\Delta J_2 \times 10^6$	-49.42	-35.40	-8.38
$\Delta J_4 \times 10^6$	23.26	17.59	4.17
$\Delta J_6 \times 10^6$	-11.12	-7.83	-1.68
$\Delta J_8 \times 10^6$	2.74	1.70	0.21
$\Delta J_{10} \times 10^6$	-0.07	0.43	0.24
$\Delta J_{12} \times 10^6$	-0.39	-0.69	-0.21
$\lvert\Delta J_{2,2}\rvert \times 10^6$	3.35	1.41	0.25
$\lvert\Delta J_{4,2}\rvert \times 10^6$	0.29	0.12	0.02
$\lvert\Delta J_{6,2}\rvert \times 10^6$	0.02	0.01	–

Notes: J_n, up to $n = 12$, caused by the axially symmetric zonal winds for the three depth parameters $R_H = 0.6641\,R_\mathrm{S}, 0.8\,R_\mathrm{S}$ and $0.90\,R_\mathrm{S}$ on the rotationally distorted Saturn; the non-axisymmetric coefficients ΔJ_{mn} are produced by convective columnar rolls with azimuthal wavenumber $m = 2$.

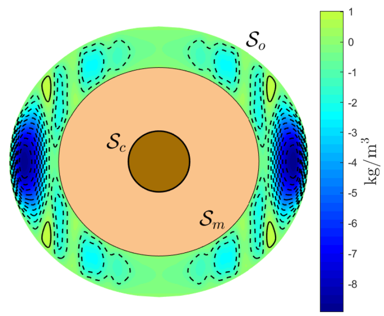

Fig. 3 The density anomaly $\rho'(\boldsymbol{r})$ in a meridional plane caused by the zonal flow confined between the molecular-metallic interface $\mathcal{S}_\mathrm{m}$ and the 1-bar pressure surface $\mathcal{S}_\mathrm{o}$ with $R_H = 0.6641\,R_\mathrm{S}$.

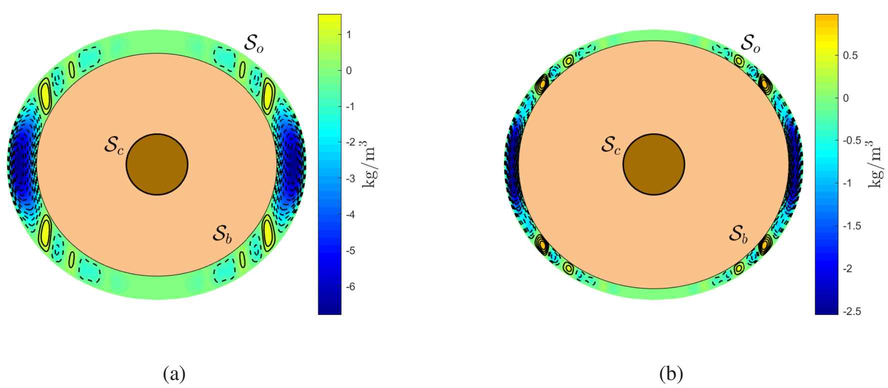

Fig. 4 The density anomaly $\rho'(\boldsymbol{r})$ in a meridional plane caused by the zonal winds confined between the constant density surface $\mathcal{S}_\mathrm{b}$ and the 1-bar pressure surface $\mathcal{S}_\mathrm{o}$ for two different cases: (a) $R_H = 0.8\,R_\mathrm{S}$ and (b) $R_H = 0.9\,R_\mathrm{S}$.

while the effect of the zonal winds on the low-order coefficients is weak with $|\Delta J_n/J_n| < \mathrm{O}(1)\%$ for $n = 2, 4$, it becomes substantial for the higher-order zonal coefficients. In particular, the coefficient at $n = 12$ with $|\Delta J_{12}/J_{12}| > 100\%$ is dominated by the redistribution of mass produced by the deep zonal winds.

The density anomalies $\rho'(\boldsymbol{r})$ for the other two cases $R_H = 0.80\,R_\mathrm{S}$ and $R_H = 0.90\,R_\mathrm{S}$ are presented in Figure 4(a,b). Compared to the density anomaly with $R_H = 0.664\,R_\mathrm{S}$, the amplitude of the density anomaly $\rho'(\boldsymbol{r})$ reduces to the maximum value of about $6\,\mathrm{kg\,m^{-3}}$ for the case $R_H = 0.80\,R_\mathrm{S}$ and, then, further to $2\,\mathrm{kg\,m^{-3}}$ for the case $R_H = 0.90\,R_\mathrm{S}$, but the cylindrical structure still remains in the domain of the flow. Figure 4(a,b) also shows that the solution $\rho'(\boldsymbol{r})$ of Equations (10)–(11) is significantly influenced by the location of the interface $\mathcal{S}_\mathrm{b}$ where the boundary conditions from Equation (13) must be satisfied. Comparing Table 1 to Table 2 in Kong et al. (2018) reveals again that the variation of ΔJ_n for $n = 2, 4$ in the cases $R_H = 0.80\, R_\mathrm{S}$ and $R_H = 0.90\, R_\mathrm{S}$ is insignificantly small, but it becomes substantial at $n = 12$ with $|\Delta J_{12}/J_{12}| > 100\%$. This implies that determining the depth of the Saturnian equatorially symmetric zonal flow via the axisymmetric gravitational field requires highly accurate modeling.

We now discuss the effect of the non-axisymmetric convective rolls on the Saturnian gravitational field. Since the gravitational signature of the non-axisymmetric flow is not directly affected by rotational distortion, the size of the coefficients ΔJ_{mn} offers a clear window for measuring the depth of the Saturnian convection in the molecular region. In other words, the non-axisymmetric gravitational perturbation, in contrast to the axisymmetric one, can be readily discerned from the gravitational anomalies caused by both the rotational flattening and the axially symmetric flow. Our fully three-dimensional computation is for the case of a large horizontal scale of the convective rolls marked by the azimuthal wavenumber $m = 2$ with the typical speed $\mathcal{U}_0 = 10\,\mathrm{m\,s^{-1}}$. The total radial gravitational anomalies – which are produced by both the axisymmetric zonal winds $U_\phi(r,\theta)$ and the prescribed convective rolls $\boldsymbol{U}(r,\theta,\phi)$ in Equation (10) – on the spherical surface of the radius $r = R_\mathrm{S}$,

$$g_r = \hat{\boldsymbol{r}} \cdot \boldsymbol{g}' = -\left(\frac{\partial V'}{\partial r}\right)_{r=R_\mathrm{S}},$$

in the exterior of Saturn are presented in Figure 5 for the case with $R_H = 0.664\, R_\mathrm{S}$. The corresponding gravitational coefficients are given in Table 1. It can be seen that the non-axisymmetric gravitational anomalies are characterized by the azimuthal wavenumber $m = 2$, largely dominated by the two spherical harmonics, Y_2^2 and Y_4^2, and have magnitude $\mathrm{O}(0.1)$ gal. We also compute the two shallow cases with $R_H = 0.8\, R_\mathrm{S}$ and $R_H = 0.9\, R_\mathrm{S}$ using the same pattern of the rolls, the results of which are given in Figure 6 and Table 1. As expected, the gravitational anomalies are still characterized by the azimuthal wavenumber $m = 2$ and dominated by the two spherical harmonics Y_2^2 and Y_4^2, but the amplitude of the gravitational anomalies reduces to $\mathrm{O}(0.01)$ gal for $R_H = 0.9\, R_\mathrm{S}$. The most significant feature is that the size of the non-axisymmetric gravitational coefficients ΔJ_{mn} directly reflects the depth of the Saturnian thermal convection while the scale of the gravitational anomalies is directly associated with the dominant wavenumber of the convective flow taking place in the interior of Saturn.

4 SUMMARY AND REMARKS

In this paper, we have employed a self-consistent perturbation approach to study the effect of the equatorially symmetric zonal winds of Saturn on its gravitational field. Since the leading-order problem accounts exactly for rotational distortion, this approach allows us to identify the variation of the gravitational field solely caused by the zonal winds. We have assumed that the fluid motion $\boldsymbol{u}(\boldsymbol{r})$ in the Saturnian interior consists of the two major components: the axially symmetric and equatorially symmetric zonal flow which is uniquely determined by the observed cloud-level winds and the non-axisymmetric columnar convective rolls which are parameterized in our model. We have calculated both the variation $\Delta J_n, n = 2, 4, 6\ldots$ caused by the axisymmetric zonal flow and the value of ΔJ_{nm} produced by the columnar rolls with $m = 2$. We have studied three different cases with penetration depth parameters $R_H = 0.644\, R_\mathrm{S}, R_H = 0.8\, R_\mathrm{S}$ and $R_H = 0.9\, R_\mathrm{S}$. We have revealed that the high-degree coefficient J_{12} is always dominated by the effect of the zonal flow with $|\Delta J_{12}/J_{12}| > 100\%$ and, more significantly, that the size of ΔJ_{mn} can directly reflect the depth and scale of the non-axisymmetric convective flow.

This paper is the second in a series on the gravitational field, shape and zonal winds of Saturn. The assumption that the cloud-level zonal winds extend on the cylinders into the interior of Saturn allows us to obtain the exact solution of Equations (10)–(11) subject to the physical boundary condition Equation (13) on the irregular surfaces $\mathcal{S}_\mathrm{b}$ and $\mathcal{S}_\mathrm{o}$. In this approach, we have to exclude the equatorially antisymmetric component of the Saturnian gravitational field. Since the rotational distortion does not contribute to the equatorially antisymmetric gravitational field (the odd zonal gravitational coefficients J_{2n+1}), this component provides a direct window into the amplitude and structure of the internal flow. Furthermore, the effect of non-spherical geometry $\mathcal{S}_\mathrm{o}$ becomes less significant for the equatorially antisymmetric component. In the third paper of this series, we will present a gravitational model of Saturn that can be used to interpret and understand its odd gravitational coefficients when they become available.

Our fully three-dimensional model discussed in this paper offers a unique means of not only interpreting the signature of the non-axisymmetric gravitational field from the measurements of the Cassini Grand Finale or some future Saturn orbiter but also understanding the

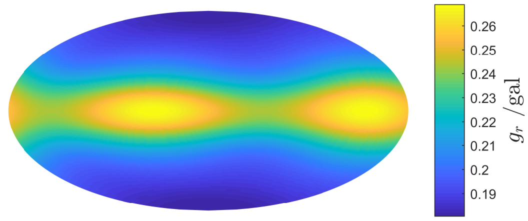

Fig. 5 The radial non-axisymmetric gravitational anomalies $g_r = \hat{\boldsymbol{r}} \cdot \boldsymbol{g}'$ in the exterior of Saturn at the spherical surface $r = R_{\rm S}$, using an equal-area (Hammer) projection, produced by the fluid motion $U_\phi(r,\theta)\hat{\boldsymbol{\phi}} + \boldsymbol{U}(r,\theta,\phi)$ confined between the molecular-metallic interface $\mathcal{S}_{\rm m}$ and the 1-bar pressure surface $\mathcal{S}_{\rm o}$.

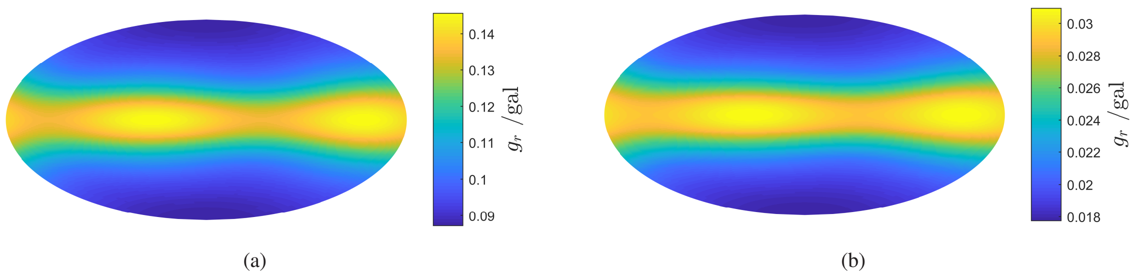

Fig. 6 The radial non-axisymmetric gravitational anomalies $g_r = \hat{\boldsymbol{r}} \cdot \boldsymbol{g}'$ in the exterior of Saturn at the outer spherical surface $r = R_{\rm S}$, using an equal-area (Hammer) projection, produced by the fluid motion $U_\phi(r,\theta)\hat{\boldsymbol{\phi}} + \boldsymbol{U}(r,\theta,\phi)$ confined between the molecular-metallic interface $\mathcal{S}_{\rm b}$ and the 1-bar pressure surface $\mathcal{S}_{\rm o}$ for two different locations of $\mathcal{S}_{\rm b}$: (a) $R_H = 0.8\,R_{\rm S}$ and (b) $R_H = 0.9\,R_{\rm S}$.

physics and dynamics of the deep Saturnian convection. Of the two key physical parameters in our convection model, the typical amplitude $\mathcal{U}_0$ contains information about the sizes of the supercritical Rayleigh number and the Ekman number in the Saturnian interior while the dominant azimuthal wavenumber m reveals a key characteristic of the deep turbulent flow. Moreover, our model, which can be readily extended to include a wide range of the spectrum for various azimuthal wavenumbers, provides an effective way of probing the three-dimensional dynamics of Saturn's interior as an inverse problem by comparing the computed external gravitational field such as that shown in Figure 5 to the non-axisymmetric high-precision gravitational measurements of Saturn.

Acknowledgements KZ is supported by Leverhulme Trust Research Project Grant RPG-2015-096, by STFC Grant ST/R000891/1 and by Macau FDCT grants 007/2016/A1 and 001/2016/AFJ. DK is supported by 1000 Youth Talents Programme of China. The computation made use of the high performance computing resources in the Core Facility for Advanced Research Computing at SHAO, CAS.

References

Busse, F. H. 1976, Icarus, 29, 255
García-Melendo, E., Pérez-Hoyos, S., Sánchez-Lavega, A., & Hueso, R. 2011, Icarus, 215, 62
Gastine, T., & Wicht, J. 2012, Icarus, 219, 428
Heimpel, M., Aurnou, J., & Wicht, J. 2005, Nature, 438, 193
Helled, R., Galanti, E., & Kaspi, Y. 2015, Nature, 520, 202
Hubbard, W. B. 1999, Icarus, 137, 357
Ingersoll, A. P., & Cuzzi, J. N. 1969, Journal of Atmospheric Sciences, 26, 981
Jones, C. A., & Kuzanyan, K. M. 2009, Icarus, 204, 227
Kaspi, Y., Hubbard, W. B., Showman, A. P., & Flierl, G. R. 2010, Geophys. Res. Lett., 37, L01204
Kong, D., Liao, X., Zhang, K., & Schubert, G. 2013, Icarus, 226, 1425
Kong, D., Zhang, K., & Schubert, G. 2016, ApJ, 826, 127
Kong, D., Zhang, K., Schubert, G., & Anderson, J. 2018, RAA (Research in Astronomy and Astrophysics), 18, 38
Liu, J., Goldreich, P. M., & Stevenson, D. J. 2008, Icarus, 196, 653
Liu, J., Schneider, T., & Fletcher, L. N. 2014, Icarus, 239, 260
Williams, D. R. 2016, Saturn Fact Sheet, *https://nssdc.gsfc.nasa.gov/planetary/factsheet/saturnfact.html*
Zhang, K. 1992, Journal of Fluid Mechanics, 236, 535
Zhang, K., & Schubert, G. 2000, Annual Review of Fluid Mechanics, 32, 409
Zhang, K., Kong, D., & Schubert, G. 2017, Annual Review of Earth and Planetary Sciences, 45, 419